Biogeochemical timescales of climate change onset and recovery in the North Atlantic interior under rapid atmospheric CO_2 forcing

Leonardo Bertini[1,2], Jerry Tjiputra [3]

[1] University of Bergen, Faculty of Mathematics and Natural Sciences, Department of Biological Sciences, Bergen, Norway

[2]Ghent University, Marine Biology Research Group, Krijgslaan 281, B-9000, Gent, Belgium

[3]NORCE Norwegian Research Centre, Bjerknes Centre for Climate Research, Bergen, Norway

Corresponding author: Jerry Tjiputra (jetj@norceresearch.no)

Key Points:

- Projections reveal complex and spatially heterogeneous responses of interior biogeochemical drivers to strong CO2 increase and mitigation

- In many parts of the North Atlantic interior, detectable anthropogenic change signals occur earlier than in the upper ocean

- In regions of relatively rapid change, interior recoveries are slower than at surface domains, mediated by changes from the South Atlantic.

Plain language summary

Widespread climate change and increasing CO_2 emissions have effects that go beyond the ocean surface, impacting ecosystems in the deep ocean. However, the timing of changes is poorly understood, let alone where particularly responsive or unresponsive areas occur following mitigation towards Pre-Industrial atmospheric CO_2. We use a computer model called NorESM to simulate the planet and its major physicochemical, geological and biological processes in the atmosphere, hydrosphere and lithosphere. We forced the model with strong and steady injection followed by strong removal of atmospheric CO_2 back to Pre-Industrial levels to understand the responses of seawater properties in the North Atlantic interior (Temperature, pH and Dissolved Oxygen). We find that southern portions of the North Atlantic interior remained up to 50% warmer and inhospitable to calcifying organisms even after returning the atmosphere to the Pre-Industrial state and allowing time for the oceans to readjust. A counterintuitive accumulation of oxygen in the ocean interior is also observed, despite reduced solubility in warmer seawater temperatures, mainly driven by reduced export and consumption of organic matter at depth. Further studies are needed to better understand the impact of anthropogenic climate change mitigation strength to safeguard the ecosystems of the deeper parts of our oceans.

Abstract

Anthropogenic climate change footprints in the ocean go beyond the mixed layer depth, with considerable impacts throughout mesopelagic and deep-ocean ecosystems. Yet, little is known about the timing of these environmental changes, their spatial extent, and the associated timescales of recovery in the ocean interior when strong mitigation strategies are involved. Here, we simulate idealized rapid climate change and mitigation scenarios using the Norwegian Earth System Model (NorESM) to investigate timescales of climate change onset and recovery and the extent of change in the North Atlantic (NAtl) interior relative to Pre-industrial (PI) variability across a suite of environmental drivers (Temperature – T; pH; Dissolved Oxygen – DO; Apparent Oxygen Utilization - AOU; Export Production - EP; and Calcite saturation state - Ω_c). We show that, below the subsurface domains, responses of these drivers are asymmetric and detached from the anthropogenic forcing with large spatial variations. Vast regions of the interior NAtl experience detectable anthropogenic signal significantly earlier and over a longer period than those projected for the subsurface. In contrast to surface domains, the NAtl interior remains largely warmer relative to PI (up to +50%) following the mitigation scenario, with anomalously lower EP, pH and Ω_c (up to -20%) south of 30°N. Oxygenation in the upper mesopelagic of up to +20% is simulated, mainly driven by a decrease in consumption during remineralization. Our study highlights the need for long-term commitment focused on pelagic and deep-water ecosystem monitoring to fully understand the impact of anthropogenic climate change on the North Atlantic biogeochemistry.

Keywords: ESM, oxygenation, Biogeochemistry, climate change, mesopelagic North Atlantic, time of emergence, recovery timescales, marine ecosystem

1. Introduction

Ocean biogeochemistry is expected to change because of future climate change, with apparent consequences for marine ecosystem services that are essential for human well-being [*IPCC*, 2019]. These changes are a result of direct and indirect impacts on the climate system and involve not only warming due increasing greenhouse gases but also subsequent changes in the large-scale circulation of the global ocean. Many studies investigating future climate change projections have highlighted that it is not just the surface and subsurface layers of the oceans which are subject to significant change because of anthropogenic forcing. The ocean interior is also affected by either direct or indirect effects of global warming as the oceans become more stratified and the main gateways for deep ocean ventilation and rates of heat and carbon sinks are compromised [*Caesar et al.*, 2020; *Gehlen et al.*, 2014; *Sarmiento and Le Quere*, 1996].

The North Atlantic (NAtl) is one of the regions of great interest to study the long-term effects of climate change given its close coupling with the atmosphere. Responses of ocean biogeochemistry to climate change are expected to be particularly stronger in zones of deep convection of the NAtl with cascading effects throughout the ocean interior via changes in the Atlantic Meridional Overturning Circulation (AMOC). The thermohaline circulation in the NAtl is largely responsible for triggering the global overturning circulation and the deep ventilation via the formation of North Atlantic Deep Water (NADW), constituting the major gateway through which anthropogenic CO_2 penetrates the interior and deep ocean on a global scale [*Tjiputra et al.*, 2010b; *Völker et al.*, 2002]. This close coupling with the atmosphere is not only strongly linked to interannual to multi-decadal climate variability [*Chen and Tung*, 2018] but also very sensitive to long-term climate change [*Goris et al.*, 2015; *Zickfeld et al.*, 2008].

Observational research suggests that the strength of the AMOC has decreased at an annual rate of 7% between 2004 and 2012 [*Smeed et al.*, 2014]. This is mainly attributed to the melting of ice caps which leads to the freshening of seawater in subduction zones. The loss of sea-ice reduces albedo, further contributing to the increase in sea surface temperature (SST), forming a positive feedback mechanism [*Box et al.*, 2012]. As a result, water column stability increases in high latitudes, which translates not only into the weakening of the AMOC but also in changes in biogeochemical properties as stratification hinders nutrient supply and affects the turnover of organic matter throughout the water column. These changes in thermohaline circulation and ocean biogeochemistry lead to decreases in ocean productivity and can ultimately disrupt marine ecosystem services that are critical to human livelihood, with impacts already evident at higher latitudes [*Wassmann et al.*, 2011]. The long-term consequences of these shifts for the global ocean carbon cycle and, in particular, the biological pump are still largely unknown, let alone the possible effects on the restructuring of biological communities in the ocean interior which depend largely on the export of particulate organic carbon (Export Production, EP) that is produced within the mixed layer [*Jones et al.*, 2014; *Ramirez-Llodra et al.*, 2011].

Habitats of the NAtl interior (i.e. the mesopelagic and deep ocean) are amongst the ones which will face the greatest challenges [*Levin and Le Bris*, 2015]. Not only do these regions depend largely on the organic matter sinking from well-lit layers, all benthic and demersal life forms in these environments have evolved in relatively stable conditions and withstand only small fluctuations in physical and biogeochemical properties, such as Temperature (T), Dissolved Oxygen (DO), Export Production (EP), and Calcite Saturation State (Ω_c). For instance, the mesopelagic NAtl is home to vast communities of cold water corals (CWC), some of which are thousands of years old and stretch out for more than 30 kilometres [*Buhl-Mortensen et al.*, 2015; *Costello et al.*, 2005]. These reefs support a diverse community of commercially important fish and associated detritivores [*Baillon et al.*, 2012; *Henry et al.*, 2013]. Furthermore, the mesopelagic ocean is also home to the largest fish communities on Earth. *Irigoien et al.* [2014] suggest that the biomass of mesopelagic fish could be 100 times greater than the global marine fisheries (~100 million tons - [FAO, 2018]).

Previous studies have focused on understanding how biogeochemical properties in the surface ocean are changing in the face of global warming and ocean acidification [*Courtney et al.*, 2017; *Kwiatkowski et al.*, 2020; *Meyer and Riebesell*, 2015; *Riebesell et al.*, 2018; *Webster et al.*, 2016] presumably because the epipelagic is the domain closest to human interactions and deep ocean species are less likely to be the first affected by changes in SST [*Coll et al.*, 2020]. However, given the importance of NAtl interior in regulating climate change and supporting life, an assessment of climate change impacts on this domain is of great relevance [*Hidalgo and Browman*, 2019]. Presently, only few studies have addressed the possible effects of climate change on the biogeochemistry and biology of the mesopelagic regions of the world's ocean [*Guinotte et al.*, 2006; *Hebbeln et al.*, 2019; *Hennige et al.*, 2015; *Puerta et al.*, 2020] and little is known about the implications of climate change recovery following the implementation of strong mitigation strategies. The timescales of climate change emergence and recovery under such scenarios are poorly understood and so are the mechanisms constraining the associated spatial variations in the interior NAtl [*Boucher et al.*, 2012].

It is important to consider that measures limiting future anthropogenic warming between 1.5 and 2°C above preindustrial levels are unlikely to be realized considering current carbon emissions and the short time span for adjustment with respect to carbon-free societal and economical transformations [*Friedlingstein et al.*, 2014; *Hofmann et al.*, 2019; *Smith et al.*, 2016; *Steffen et al.*, 2018]. Under this perspective, addressing ecosystem recovery using mitigation scenario in Earth System Models is necessary since the most representative scenarios towards achieving the current Paris Agreement target would involve negative emissions [*Gasser et al.*, 2015; *Tokarska and Zickfeld*, 2015]. Therefore, assessing the extent with which the biogeochemistry of the NAtl interior will shift and whether mesopelagic ecosystems would be able to recover under such mitigation is fundamental if we are to aim for a manageable future in the framework of a Blue Economy. This will allow us to better understand the extent of interior ocean change and the subsequent effects of such a transition on marine ecosystem drivers.

Here, we analyse the biogeochemical responses from an idealized climate change scenario of rapid warming followed by rapid cooling in the NAtl interior simulated by an IPCC-class Earth System Model. Our main objective is to evaluate the spatio-temporal evolution of key ecosystem drivers of temperature, ocean acidity, dissolved oxygen, particulate organic carbon export, and calcite saturation state (T, pH, DO, EP and Ω_c respectively) throughout the different phases of the simulation and the reversibility of these drivers following a strong mitigation scenario and allowing for the system to readjust after returning atmospheric CO_2 (CO_{2atm}) back to preindustrial levels. More specifically, we determine: 1) the timescales associated with the onset of anthropogenic signal, 2) the extent of change throughout the different simulation phases and 3) the persistence as well as the reversibility of the anthropogenic signal after applying mitigation, focusing on the dynamics of the North Atlantic Meridional Overturning Circulation and large-scale biogeochemical feedbacks.

2. Material and Methods

2.1 Model system: a short overview

We employ the Norwegian Earth System Model (NorESM1-ME; *Tjiputra et al.* [2013]), which consists of atmospheric, ocean, sea-ice and land modules. The horizontal resolution of atmospheric and continental domains is ~2° whilst that of oceanic and sea ice is ~1°. The atmospheric component is derived from the Oslo version of the NCAR Community Atmosphere Model (CAM4-Oslo; [*Kirkevåg et al.*, 2012]). The physical oceanic component is a modified version of the Miami Isopycnic Coordinate Ocean Model (MICOM; *Bentsen et al.* [2013]). The biogeochemical ocean module is originated from the Hamburg Oceanic Carbon Cycle model (HAMOCC; [*Maier-Reimer*, 1993]), and adapted to an isopycnic framework [*Assmann et al.*, 2010; *Tjiputra et al.*, 2010a; *Tjiputra et al.*, 2013]. A full description and evaluation of the NorESM1-ME are available in *Bentsen et al.* [2013] and *Tjiputra et al.* [2013] respectively. A brief description of relevant representations of biogeochemical process in the model are provided in the Supporting Information.

2.2 Experiment design

Prior to any external forcing, NorESM1-ME was spun up under a preindustrial (PI) condition (constant 284.7 ppm CO2atm) for 900 years, allowing for a quasi-equilibrium state with a weak climate drift. Initial conditions for oxygen and nutrient fields were derived from the World Ocean Atlas (WOA; [Garcia et al., 2010a; Garcia et al., 2010b]), whereas dissolved inorganic carbon and total alkalinity values were obtained from the Global Data Analysis Project (GLODAP) data set [Key et al., 2004]. The remaining biogeochemical variables in the water column are either set to zero or small but non-zero values. Further information on the spin-up phase of NorESM can be found in [Tjiputra et al., 2013]. After the spin-up phase, two simulations were performed: (i) a PI control (CTRL) and (ii) an anthropogenic climate change simulation.

The CTRL simulation encompasses 250 model years at a PI state. The anthropogenic simulation consists of three subsequent transient phases: Ramp-up, Ramp-down and Extension. During the Ramp-up, CO2atm is increased at a rate of 1% yr-1 from the PI CO2atm level for 140 years, reaching approximately four times the PI mean value. The Ramp-down illustrates an idealized scenario of rapid negative emissions where CO2atm is reduced at a mirroring rate of -1% yr-1 for another 140 years, returning to the PI baseline. This annual rate of decrease follows the standard protocol of the Carbon Dioxide Removal Model Intercomparison Project (CDRMIP [D P Keller et al., 2018]). The Extension phase involves extending the anthropogenic simulation for 200 years from the end of Ramp-down (Fig. 1a), where CO2atm is kept at the PI value to determine the long-term responses.

Although these changes in CO_{2atm} may seem very rapid and unrealistic when compared to the observed rate [*Keeling et al.*, 2005], they are employed to induce strong anthropogenic forcing so that anthropogenic climate change signals, both in terms of departures and recoveries, can manifest as early as possible (e.g., *Schwinger and Tjiputra* [2018]). Therefore, the results from this idealized scenario constitute an important tool for assessing not only the upper limits of climate change onset and climate change recovery but also the inertial responses involved in the biogeochemistry of the interior ocean over different phases of transitional forcing.

2.3 **Post-processing**

Here, we interpolate the NorESM1-ME outputs from its native isopycnal vertical coordinate to regular vertical level fields (see supplementary material for more information on the interpolation and Table S1 for a list of output variables used in the study). Since the objective of this study is to understand the onset timescales and the extent of recovery in response to anthropogenic forcing, the monthly-to-seasonal variability is not of interest. We have therefore converted all monthly biogeochemical fields into annual fields.

Apparent Oxygen Utilization (AOU) was determined by subtracting dissolved oxygen (DO) outputs from the estimated saturation concentration (O_{2sat}), determined using T and S fields and a MATLAB 2018b routine based on functions from the Gibbs SeaWater (GSW) Oceanographic Toolbox [*McDougall and Barker*, 2011].

2.4 Timescale analyses

Prior to conducting any timescale analyses, timeseries for all variables were corrected for model drift by subtracting the trends in the CTRL run from the anthropogenic runs. The time-related variables presented in this study were estimated for each grid box in the model. For each grid box, a range of natural variability in time was defined as two times the standard deviation of the last 30-yr period of the CTRL run (2*PIsd30). This envelope (±2*PIsd30) represents the natural variability range of the respective variables (T, S, DO, etc.), meaning that any sustained deviation outside this envelope during the climate change simulation originates from external anthropogenic forcing.

Our predefined natural envelope had at its centre the mean from the last 5 years of the Pre-industrial field in question (PImean5) and its upper and lower limits are given by PImean5 ± 2*PIsd30. All time-scale variables were calculated using MATLAB 2018b routines (see Supporting Information).

To test how sensitive the timescales were to the adopted envelope, we have also computed timescales based on different envelope widths, i.e., PImean5 ± 1*PIsd30 and PImean5 ± 3*PIsd30. The envelope based on a fluctuation of ± 1*PIsd30 represents a more restricted condition, where departures occur earlier and recoveries later. Oppositely, the envelope based on a fluctuation of ± 3*PIsd30 represents a more tolerant condition, where departures occur later and recoveries earlier (see examples in Fig. S1).

2.4.1 Time of Departure (ToD)

ToD is a concept similar to ToE (Time of Emergence, [*Henson et al.*, 2017; *Keller et al.*, 2014; *Tjiputra et al.*, 2018]). We used the terminology 'Time of Departure' because our analyses are based on a perspective where transient variability leaves predefined envelopes of natural variability. ToD is defined in our study as the point in time when there are at least 10 consecutive and non-returning model years outside the predefined envelope. ToD indicates the onset of the detectable anthropogenic signal when a particular grid point is exposed to conditions outside its PI natural variability.

2.4.2 tmax and $Tracer_{tmax}$

The point in time when the series reaches its minimum or maximum change after the start of the Mitigation phase (i.e., Ramp-down) is given by tmax. This can be understood as the turnaround point marking the onset of the mitigation phase (i.e., from model year 140, which is when the CO_{2atm} begins to decline). In the case of pH and DO, it is expected that tmax represent the time of the global minima, since these variables are expected to decrease with climate change and increasing CO_{2atm}, whereas for T, tmax represents the time of maximum warming. The values associated with tmax are given by $Tracer_{tmax}$, which is the maximum or minimum value experienced at a grid point over the entire simulation period.

2.4.3 Trec

When the time-series re-enters the natural variability envelope within the duration of the experiment, Trec is defined as the first point in time when the series returns to the envelope and remains in it for at least 10 consecutive years. If the series does not show a sustained return of at least 10 years, a linear regression is calculated using the last 100 years of the Extension phase to estimate Trec (see examples in Fig. S2).

2.4.4 Time-slices percentage change

To identify which regions have significantly changed over the course of the anthropogenic simulation compared to the PI, statistical analyses of percentage change of both physical and biogeochemical fields were carried out using 30-year windows (paired t-tests at a significance level α=0.05). The periods compared against the last 30 years of the PI were: a) the last 30 years of the Mitigation phase (model years 250-280), b) the middle of the Extension phase (model years 350-380) and c) the last 30 years of the Extension phase (model years 450-480). Data flagging was conducted to mark where significant changes were observed with respect to the PI. More information on the test performed and the code used are available in the Supporting information.

3. Results

3.1 Basin-scale evolution

Area-weighted and volume-weighted results for the NAtl (Equator-65°N) reveal that the mean SST and the water column temperature increased by 0.13°C and 0.70°C by the end of the climate change simulation, respectively (Fig. 1b). The mean surface pH returns to the PI value while water column pH decreases by 0.025 units (Fig. 1c). The mean water column DO and AOU decrease by 1.47 μmol kg^{-1} and 3.60 μmol kg^{-1}, respectively (Fig. 1d). This suggests that warming and deoxygenation in the NAtl relative to the PI persist, even after the Extension phase.

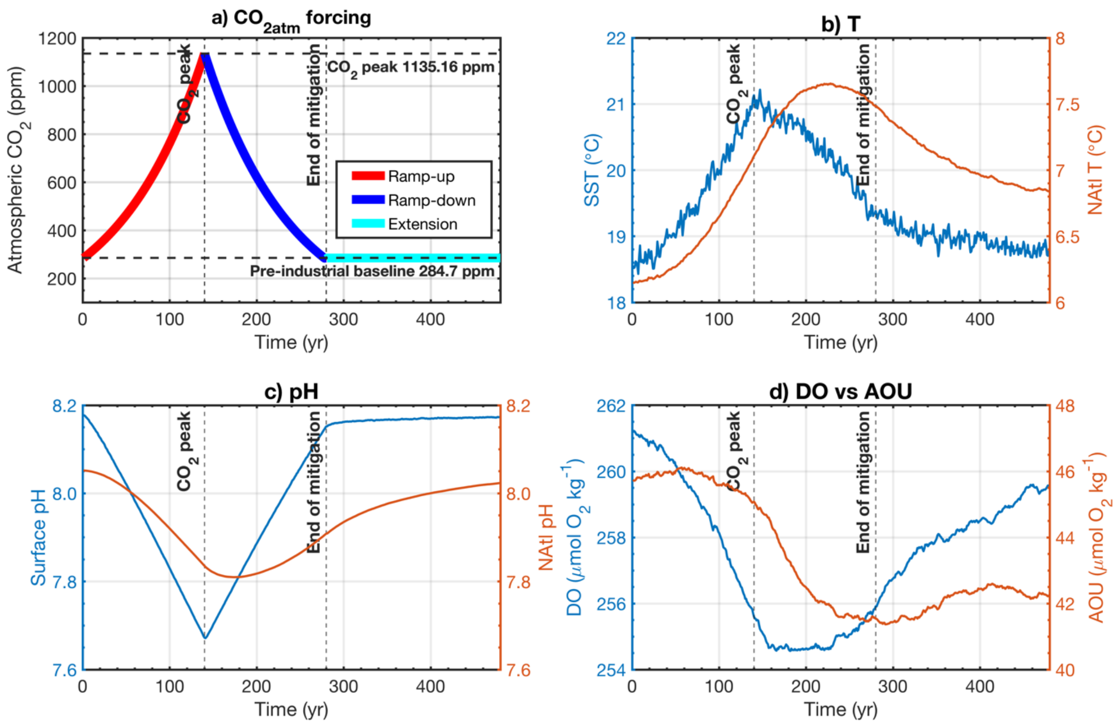

Figure 1 – Transient evolution of **a)** prescribed atmospheric CO_2 forcing; North Atlantic **b)** area-weighted mean sea surface temperature (SST) in blue and volume-weighted mean water column temperature (NAtl T) in orange; **c)** area-weighted mean seawater surface pH in blue and volume-weighted mean water column pH in orange and **d)** volume-weighted water column mean Dissolved Oxygen (DO) in blue and Apparent Oxygen Utilization (AOU) in orange.

The evolution of the mean T vertical profile shows that thermal stratification in the mesopelagic NAtl is more pronounced 100 years after the peak of CO_{2atm} (Fig. 2a). Our results suggest an increase in T by as much as +3°C between 500 m and 2000 m depths. At the end of the simulation, isotherms in the deep mesopelagic NAtl are still shifted deeper by more than 500 m from their PI position and by more than 1000 m in the deep NAtl. The evolution of the mean pH vertical profile shows that the upper mesopelagic NAtl would experience pH values as low as 7.6 for a sustained period of more than 100 years (between model years 120 and 240), a ΔpH of -0.4 relative to PI levels. Changes in the interior NAtl down to 2000 m for the same period are also pronounced, with pH values as low as 7.7, which also corresponds to a ΔpH of -0.4 (Fig. 2b).

Regarding the evolution of the mean DO vertical profile, the expansion of the oxygen minimum zone is evident in the upper mesopelagic NAtl up to model year 300, where levels remained as low as 100 µmol kg^{-1}. Deep ventilation at the base of the mesopelagic NAtl is compromised during the Ramp-up, with a sustained signal of deoxygenation at depths >2000 m. However, when it comes to depths between 1500 m and 2000 m, it is evident that after model year 180 there is an oxygenation trend (Fig. 2c), with an apparent shallowing of oxygen isolines (see discussion).

The evolution of the mean AOU vertical profile up to model year 200 shows a relative increase in the deep NAtl (between 2000 m and 4000 m) when compared to PI levels. From model year 200, however, our results indicate a decrease in AOU at depths between 1000 m and 2000 m, which is linked to the enhanced ventilation associated with a rebound of AMOC strength (oxygenation is also detected in the same period). From model year 300, AOU levels in the deeper mesopelagic NAtl (roughly at 2000 m deep) reach their lowest values (Fig. 2d).

The evolution of the mean Ω_c vertical profile shows that the deep ocean calcite lysocline reaches its shallowest position during model year 140, coinciding with the peak of CO_{2atm} (Fig. 2e). In the upper mesopelagic (between 500 m and 1000 m), conditions favouring calcite dissolution start to arise from model year 120 and persist throughout the duration of the simulation. In the middle of the mesopelagic (1500 m deep), conditions favouring calcite dissolution arise ~80 years later and persist until model year 400.

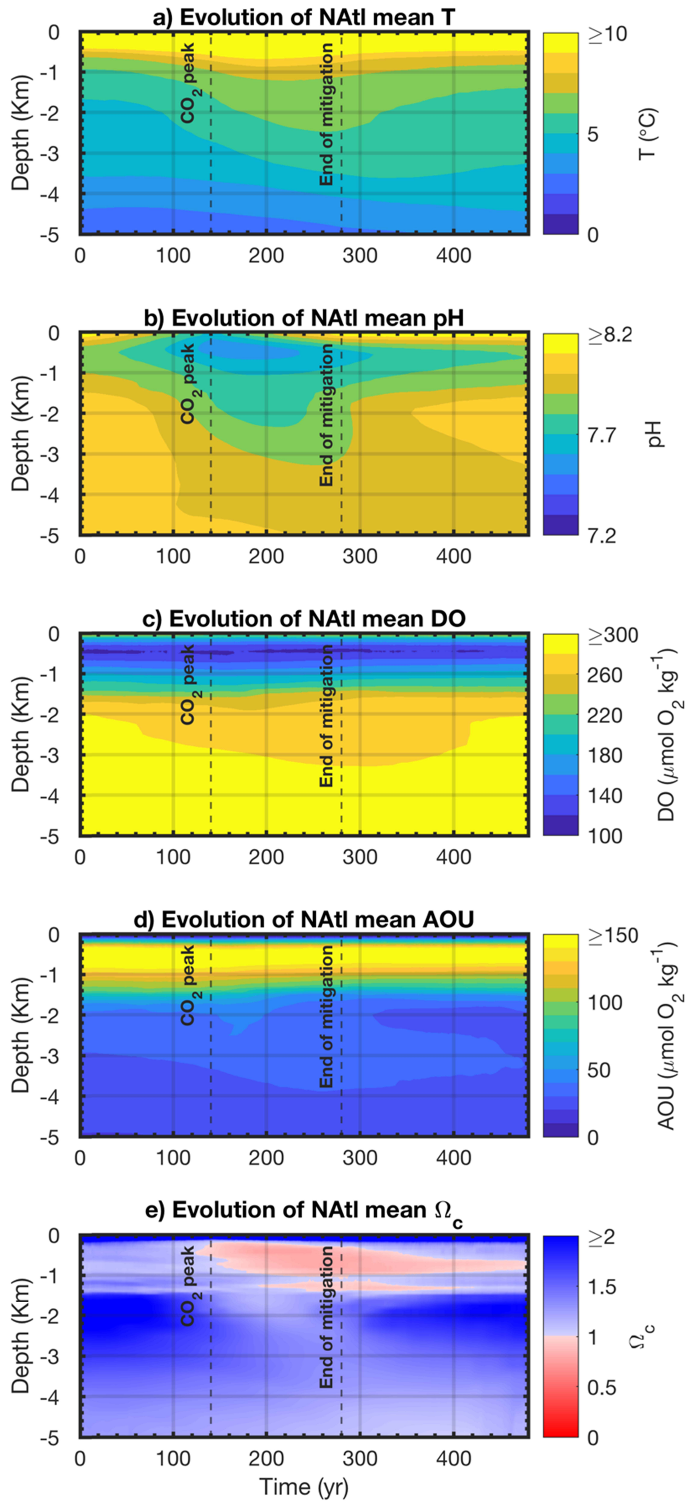

Figure 2 – Temporal evolution of mean vertical profiles of volume-weighted **a)** Temperature (T), **b)** pH, **c)** Dissolved Oxygen (DO), **d)** Apparent Oxygen Utilization (AOU) and **e)** Calcite saturation state (Ω_c) throughout the simulation for the North Atlantic. Dashed vertical lines mark model year 140, when CO_{2atm} reaches its peak in the atmosphere (1135.16 ppm) and model year 280, when the mitigation trend stopped and CO_{2atm} returned to the PI baseline (284.7 ppm).

3.2 Temperature (T)

The vertical profile based on an envelope of 2PIsd suggests that the mean ToD for Temperature in the upper NAtl is highly delayed (Fig. 3a), with moderate values of ToD (60±10 yr) in the first 50 m of the water column, followed by a zone of climate change buffering down to 200 m deep encompassing the highly variable thermocline, marked by the highest ToD (85±40 yr). Below the thermocline, Temperature ToD decreases throughout the mesopelagic NAtl with values of 40±10 yr.

The meridional section along the western NAtl shows relatively later departures in the mesopelagic north of 40°N (Fig. 3c). South of 40°N, ToD values decrease throughout the mesopelagic, indicating domains that are more sensitive to climate change with respect to fluctuations in Temperature. Time of recovery (Trec) estimates show virtually no recovery within the time span of the simulation, with projected values no lower than 700 years occurring throughout most parts of the NAtl section (Fig. 3d). The exceptions were the very bottom (4500-5000 m), with Trec ranging between 300-450 years and the very surface (<200 m), where Trec values ranged between 320-400 model years. At the very surface between 45°N and 50°N, a patch of low Trec values (< 200 years) is simulated. This marks a region where a cooling trend has been detected (not shown). In this patch, temperatures up to 10% cooler are projected at the end of the Extension phase, with its position varying eastwards at depth (see Fig. S3). This feature is also present in other models [*Drijfhout et al.*, 2012], referred to as the Warming Hole (WH) (see discussion).

The model projects NAtl interior to be 15% warmer basin-wide, even after mitigating emissions and allowing for 200 years of extension time (Fig. 3b blue solid line). The top 3000 m of the water column warmed up by up to +40% after the Mitigation phase, gradually decreasing to +25% and then +15%, from simulation periods 250-280, 350-380 and 450-480 (Fig. 3b dashed green, dashed yellow and solid blue lines, respectively), showing a tendency towards recovery. On the other hand, the delayed response in the deep NAtl is evident at depths greater than 3000 m, where a gradual increase in the percentage change signal is observed from simulation period 250-280 to 450-480 (Fig.3b solid blue line reaching values of up more than 50% warmer in the deep NAtl). When looking at the vertical section at the end of the Extension phase (Fig. 3e), our results suggest significant changes of up to 20% and 50% warmer in the mesopelagic and deep Natl, respectively.

It is important to highlight that the warming signal seems to be stronger in low-latitude regions, suggesting unlikely recoveries in the deepest domains (>3000 m deep). Conversely, there is a gap in terms of significant differences in the lower mesopelagic (1000-3000 m deep; Fig. 3e) between 40°N and 60°N, which suggests eventual recoveries in this zone outside the timeframe of our simulations.

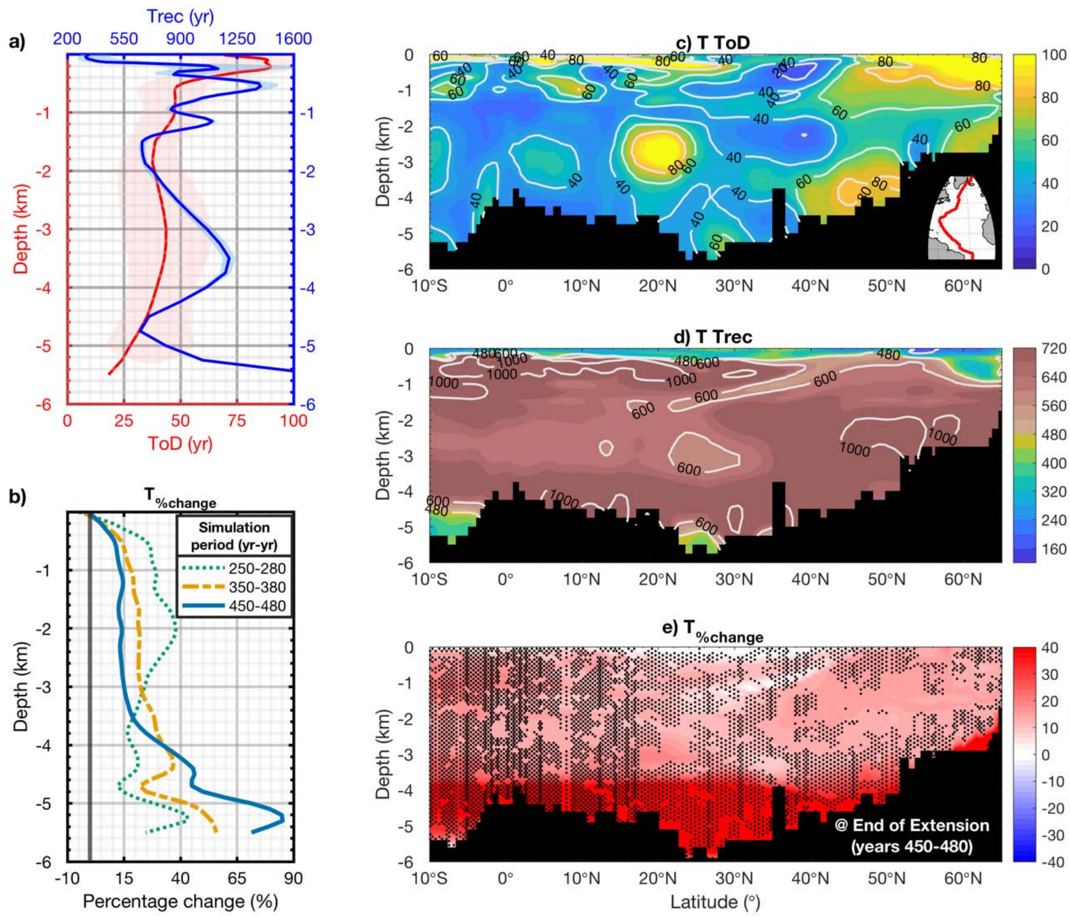

Figure 3 - North Atlantic (0-65°N) volume-weighted vertical profiles of **a)** mean Temperature ToD and Trec (yr), solid red and blue lines respectively and **b)** mean Temperature percentage change (%), across different simulation periods: years 250-280 (end of Mitigation phase), years 350-380 (halfway through the Extension phase) and years 350-380 (end of Extension phase); panels **c-e** show the meridional section along the western side of the basin (red line in panel c, bottom right corner) of temperature **c)** ToD, **d)** Trec, with brown-shaded areas indicating recovery outside the time span of the simulation (> 480 yr), and **e)** percentage change (%) at the end of Extension phase. Stippling in **(e)** indicates regions of significant differences relative to the PI values. Units in **(a, c, d)** are model years since the start of the simulation. Shading around solid lines in panel **(a)** represent uncertainty range estimated using different natural variability envelopes (see Sect. 2.4).

3.3 Dissolved Oxygen (DO)

ToD for Dissolved Oxygen (DO, Fig. 4a) and AOU (see Fig. S4) indicate an overall consistent and decreasing pattern with narrowing uncertainties at depth until the base of the mesopelagic (2000 m). Subsurface DO and AOU ToD estimates show values of 100±30 yr, whereas at 2000 m deep values are ~45±15 yr. The narrowing of the DO ToD spread reflects the relatively stable mesopelagic NAtl with respect temporal fluctuations in DO. Additionally, a feature of particularly high DO ToD values is observed at 2000-3000 m depths in 20-30°N (Fig. 4c), suggesting a highly delayed anthropogenic signal which matches the pattern observed in Fig. 3a for Temperature. These delays indicate the relatively weak influence of the NADW water mass in this region.

Trec timescales for DO increase gradually from the subsurface towards a local maximum in the mesopelagic NAtl, followed by a decrease down to 3000 m and a subsequent increase towards the deep ocean (Fig. 4a). In the subsurface down to the upper mesopelagic (1000 m), recoveries are projected to occur within the time span of our simulation (Trec < 480 years) except for two domains at the subsurface comprised between 5-10°N and 20-30°N where projected timescales of Trec seem to be at least twice as long (Fig. 4d).

In the mesopelagic NAtl between 2000-3000 m deep, recoveries are projected to occur no less than 1300 model years after the start of the Anthropogenic simulation, with two particularly high-Trec clusters, one in the equatorial region between 0-5°N and another in the subarctic domain between 50-60°N (Fig. 4d). Past 3000 m deep, the subsequent decrease in Trec is associated with likely recoveries within the time span of the simulation between 40-60°N, suggesting that the AMOC is regaining its strength and the recovery of DO towards PI levels is initiated. Overall, our results indicate that both the subsurface and the very deep domains are likely to recover before the mesopelagic domain, where a tongue of particularly high DO Trec values persists between 1000-3000 m.

Our results for DO percentage change show two contrasting domains (Fig. 4b and 4e). Regions below the NAtl mixed layer (i.e., 500-1000 m) experience an oxygenation trend of +10%, +25% and then returning to +10% relative to the PI levels from the end of Mitigation to middle of the Extension and end of Extension phases respectively. On the other hand, the mesopelagic and deep NAtl domains experience overall deoxygenation trends. The mesopelagic between 1500-2000 m is the region with the lowest DO content, decreasing by 5% at the end of Mitigation phase and regaining DO as the simulation evolved towards the end of Extension phase, where levels were ~2% lower than PI values. Conversely, the delayed response in the deep NAtl is apparent from the subsequent decreases in DO, with the highest DO change (-6%) at the end of the simulation.

It is important to highlight that the oxygenation just below the mixed layer is limited to the region south of 30°N. North of 30°N, a slight but significant trend of deoxygenation is simulated (Fig. 4e). Additionally, the gap in terms of significant differences in the mesopelagic NAtl (1000-3000 m) between 40°N and 60°N suggests eventual recoveries in this zone outside the timeframe of our simulation similar to the pattern for Temperature (Fig. 3e).

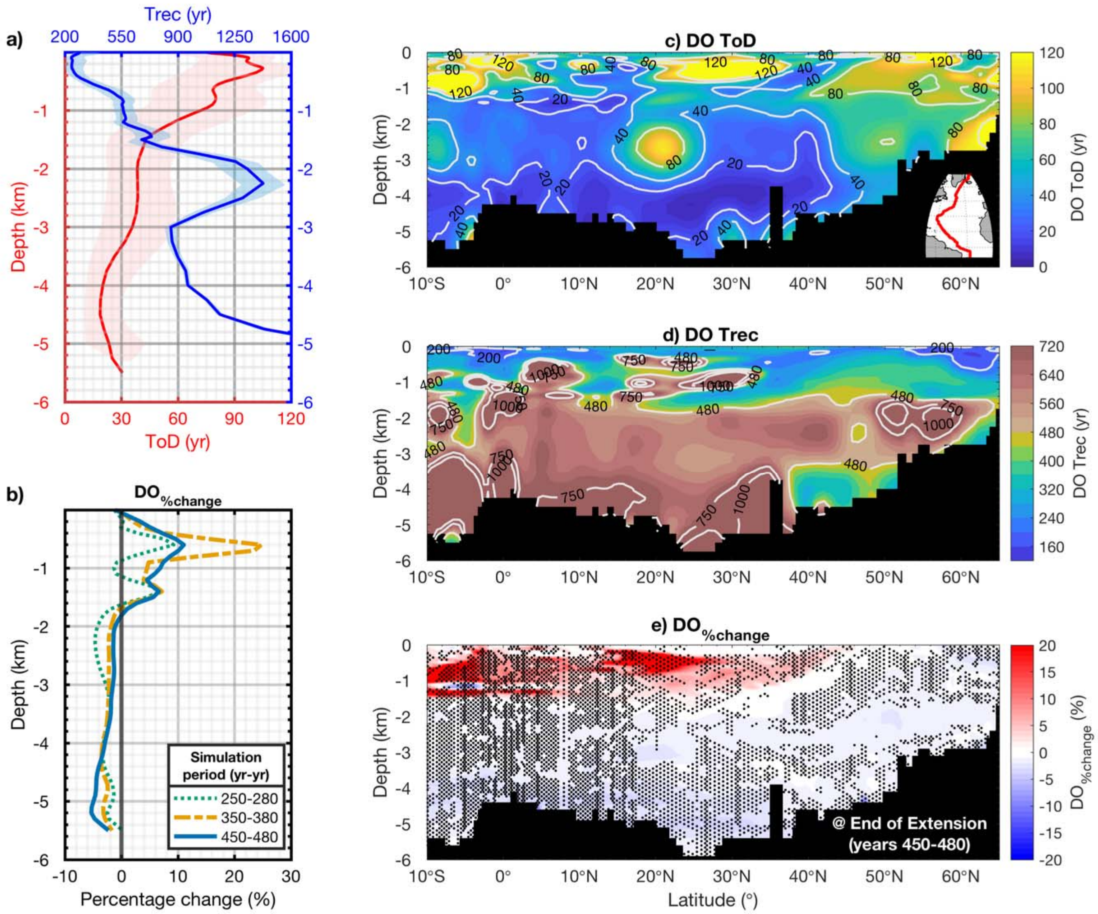

Figure 4 - North Atlantic (0-65°N) volume-weighted vertical profiles of **a)** mean DO ToD and Trec (yr), solid red and blue lines respectively and **b)** mean DO percentage change (%), across different simulation periods: years 250-280 (end of Mitigation phase), years 350-380 (halfway through the Extension phase) and years 350-380 (end of Extension phase); panels **c-e** show the meridional section along the western side of the basin (red line in panel c, bottom right corner) of DO **c)** ToD, **d)** Trec, with brown-shaded areas indicating recovery outside the time span of the simulation (> 480 yr), and **e)** percentage change (%) at the end of Extension phase. Stippling in **(e)** indicates regions of significant differences relative to the PI values. Units in **(a, c, d)** are model years since the start of the simulation. Shading around solid lines in panel **(a)** represent uncertainty range estimated using different natural variability envelopes (see Sect. 2.4).

3.4 Calcite Saturation State (Ω_c)

The onset of climate change for Ω_c can be detected throughout the water column in less than 50 years (Fig. 5a,c), correlating tightly with patterns from the pH ToD profile (see Fig. S5). The subsurface zone (0-500 m) shows the earliest departures (10±5 yr) due to the decrease in pH as a result of enhanced CO_2 uptake from the atmosphere. In the upper mesopelagic (500-1500 m deep) a relatively higher Ω_c ToD is simulated (50±15 yr), forming a buffer zone for ocean acidification. This part of the NAtl is mainly influenced by two major clusters of relatively high ToD values, between 15-30°N at ~1000 m and between 45-60°N at 1500 m (Fig. 5c). Ω_c ToD decreases gradually between 1500-3000 m, reaching practically homogeneous values within the 2500-3500 m depth range that are similar to that found at the very surface (10±5 yr). This shows not only the connectivity of this zone via deep ocean ventilation but also a very stable environment that is prone to change. In the deepest part of NAtl, the results from our simulation show a gradual increase in Ω_c ToD values.

Lower Ω_c Trec values (up to 320 years), were characteristic of the surface, between 0 and 250 m deep, and throughout the mesopelagic north of 35°N down to 2500 m depth (Fig. 5a, d). This shows that recoveries with respect to Ω_c are unlikely during the simulated Mitigation phase and are only observed some 50 years into the Extension phase. Conversely, south of 35°N, relatively late Trec values were obtained for most of the subsurface, mesopelagic and deep NAtl domains with estimates no lower than 500 years and even higher southwards (Fig. 5d). It is important to highlight the presence of a particularly high Ω_c Trec region observed between 2000-3000 m deep around 20°N, where Trec are greater than 1000 years. This region coincides with the zone of relatively early departures of Ω_c and to zones of delayed departures of DO and T.

Figure 5b shows that the period with the highest percentage change of Ω_c in the NAtl is at the end of the Mitigation phase, where saturation states decreased by more than 25%

in the entire mesopelagic (1000-3000 m) relative to PI levels. These negative changes are attenuated over time, with absolute negative changes decreasing from approximately 15% to <5% from the middle to the end of the Mitigation phase, respectively.

When looking at the last 30 model years, a significant portion of the NAtl north of 30°N is characterized by 0% change suggesting likely recoveries, both in the subsurface and at 2000 m depth (Fig. 5e). However, some regions encompassed by the meridional section show an overall significant decrease of up to -10% even at the end of the Extension phase south of 20°N, with a localized minimum of up to -20% at around 1000 m. Furthermore, north of 30°N, a small tendency towards increased calcite saturation states is simulated (up to +5%) and associated with insignificant differences between 1000-2000 m, which suggests an overall recovery followed by a minor Ω_c overshoot in the mesopelagic NAtl.

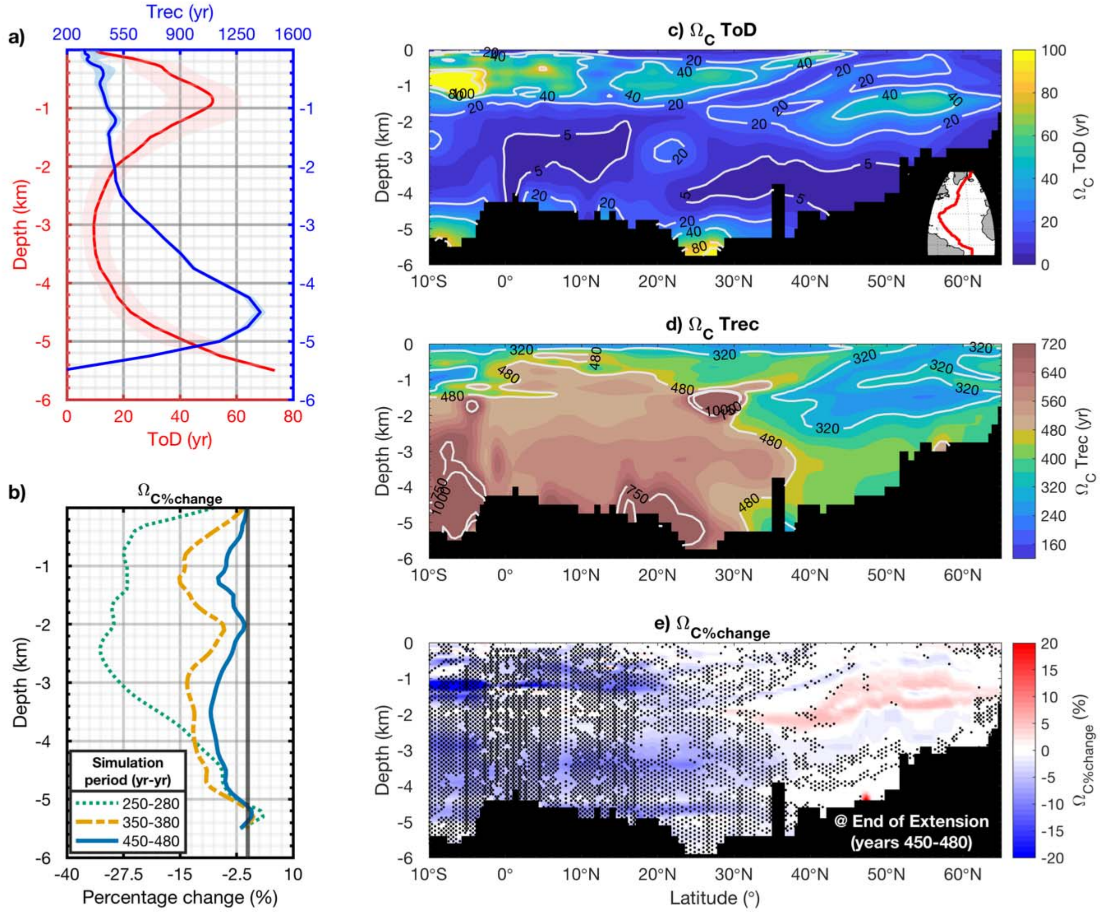

Figure 5 - North Atlantic (0-65°N) volume-weighted vertical profiles of **a)** mean Ω_c ToD and Trec (yr), solid red and blue lines respectively and **b)** mean Ω_c percentage change (%), across different simulation periods: years 250-280 (end of Mitigation phase), years 350-380 (halfway through the Extension phase) and years 350-380 (end of Extension phase); panels **c-e** show the meridional section along the western side of the basin (red line in panel c, bottom right corner) of Ω_c **c)** ToD, **d)** Trec, with brown-shaded areas indicating recovery outside the time span of the simulation (> 480 yr), and **e)** percentage change (%) at the end of Extension phase. Stippling in **(e)** indicates regions of significant differences relative to the PI values. Units in **(a, c, d)** are model years since the start of the simulation. Shading around solid lines in panel **(a)** represent uncertainty range estimated using different natural variability envelopes (see Sect. 2.4).

3.5 Export Production (EP)

Figure 6a and b shows that an expansion of the low EP area is noticeable in the subtropical gyre and the western part of the NAtl, over the Sargasso Sea domain. Conversely, at higher latitudes, there has been an intensification north of 45°N between 40-45°W, which coincides with the latitudes of WH occurrence.

The simulated EP ToD ranged between 100 and 150 years (Fig. 6c, e), or no departures at all. The zonally-averaged EP ToD revealed values of relatively early departures towards the Equator and patches of 'no departure' predominantly throughout the eastern NAtl between 30-45°N and in higher latitudes (>60°N; Fig. 6e). Late departures are found in the transition regions between the subtropical and the subpolar gyres (~180 years) and coincide with the regions with the highest natural variability such as the Labrador Sea and the WH area.

Overall EP Trec estimates reveal a homogeneous meridional distribution with mean values of ~200 years, suggesting that recovery timescales are projected to occur towards the end of the Mitigation phase. A relative increase towards lower latitudes is projected, but Trec remain lower than 250 years, indicating delayed recoveries in this region. This is mainly attributed to the high natural envelope simulated both at the Canary and western African upwelling regions (Fig. 6d). Other exceptions include the Azores and the Grand Banks off Newfoundland, where Trec were outside of our simulation period (>480 years).

Compared to the PI, EP at the end of the Mitigation phase is projected to decrease between -20% and -25%, except for a region encompassing the western part of the Irminger Sea and the domain from the Reykjanes Ridge to the Azores, where percentage change exceeded +25%, coinciding with the WH region (see Fig. S6). Both the positive and the negative changes gradually decrease over time in terms of magnitude and spatial extent. At the end of the Extension phase, our results indicated that the NAtl domain becomes largely less productive with an overall decrease in EP by up to -20% in parts of the subtropics. However, positive changes over the Azores ridge and the western Irminger Sea remain, with EP values of up to +15% higher than PI, showing some localized increase in export production over the WH region (Fig. 6f).

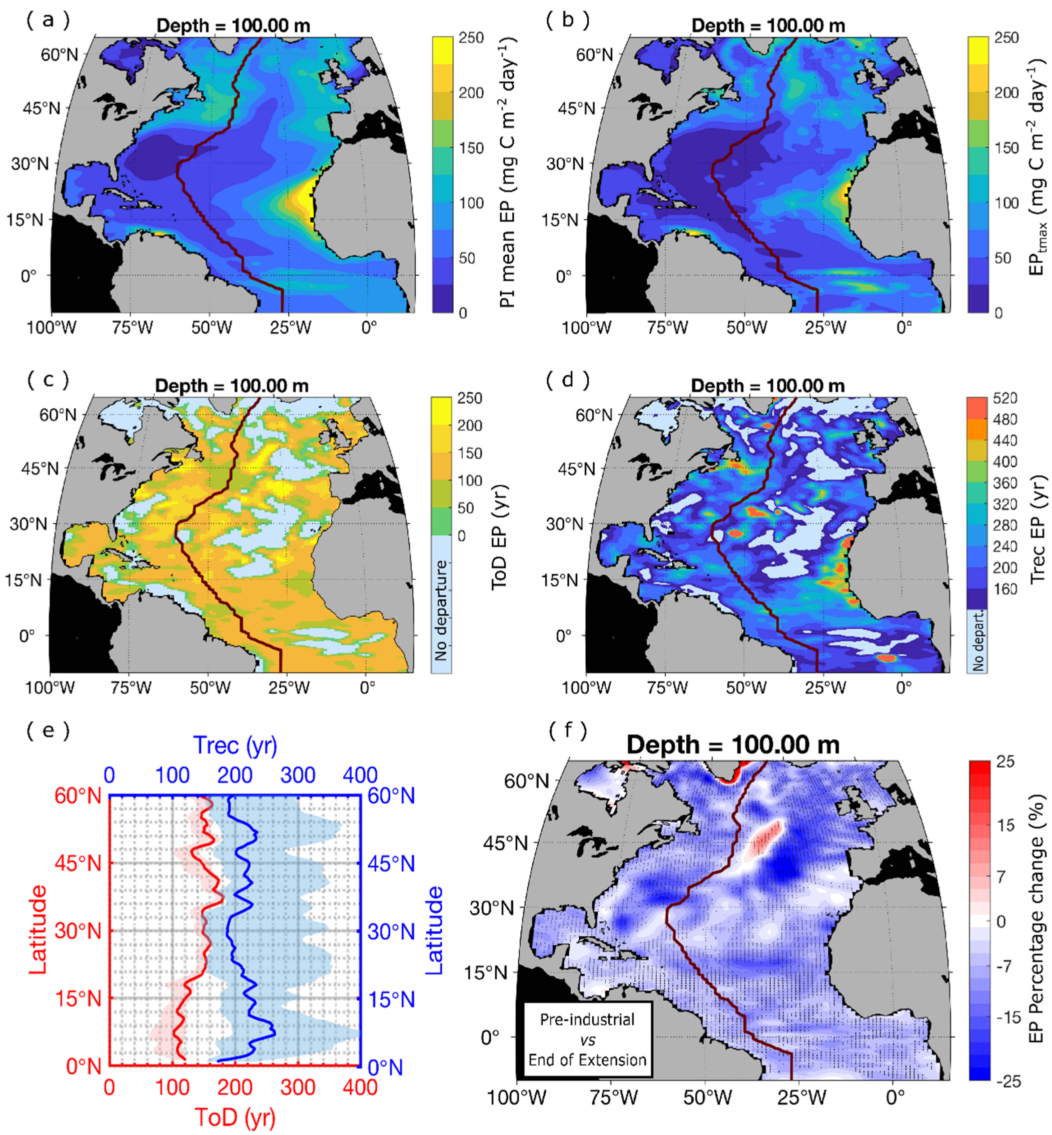

Figure 6 – Maps of **a)** Pre-industrial mean of Export Production (EP) distribution [mg C m^{-2} day^{-1}]; **b)** EP at tmax [mg C m^{-2} day^{-1}]; **c)** EP Time of Departure (ToD) and **d)** EP Time of Recovery; **e)** North Atlantic (0-65°N) zonally-averaged EP ToD and Trec (yr) and **f)** mean EP percentage change (%) at the end of Extension phase, where stippling indicates regions of significant differences. The timescale estimates are based on an envelope of 2 standard deviations with light blue areas showing regions of no departure in panels (c) and d). All year units are model years since the start of the simulation.

Shading around solid lines in panel (e) represent uncertainty range estimated using different natural variability envelopes (see Sect. 2.4).

4. **Summary and Discussion**

Temperature (T)

The delayed climate change onset (ToD) in the shallow NAtl (Fig. 3a) and, more specifically, at latitudes between 10-30°N and poleward of 50°N (Fig. 3c), indicates respectively not only subsurface water isolation in the NAtl subtropics but also that the anthropogenic signal is relatively smaller when compared to the natural variability of Temperature, especially at temperate and subarctic latitudes, highlighting the tight coupling between atmospheric variability, heat exchange and the gyre circulation. Additionally, our simulation yields maximum ToD within the thermocline zone (Fig. 3a, c), suggesting that this region can be understood as a buffer zone in terms of seawater warming. Here, a sustained long-term anthropogenic perturbation more than in any other region is needed before an evident climate change signal can be detected. A recent study by *Hameau et al.* [2019] focused on changes within the thermocline (200-600 m) under RCP 8.5 (Representative Concentration Pathways) future scenario also suggests delayed ToD for temperature around ~20°N by the end of the century within the thermocline domain, which is consistent with our results and suggests a climate change buffer zone influenced either by high natural variability or inhibited anthropogenic response or even a combination of both as also suggested in the *Hameau et al.* [2019] study. This highlights the need of further studies to better understand the biogeochemical feedbacks in the thermocline domains as well as the mixed layer under strong anthropogenic forcing.

In contrast, despite delays in temperature ToD at the domains described above, our results suggest that changes in the interior NAtl can occur as early as 40 years in our scenario of rapid atmospheric warming. Past the thermocline, the uniformly lower ToD values (Fig. 3a,c) indicate how sensitive the mesopelagic and deep NAtl zones are and how early global warming can have an impact on their ecosystems relative to the surface and subsurface layers. Furthermore, our results show that the narrowest ToD spread is simulated in the mesopelagic zone, highlighting its stable environmental condition and, consequently, its susceptibility to fluctuations in T compared to other regions of the NAtl interior.

The projected low Trec at both the deepest domains of the NAtl (4500-5000 m) and the superficial layer (<200 m) suggest that the former can be attributed to a thermohaline recovery signal brought by the AABW and the latter to a recovery in subsurface levels due to the atmospheric readjustment and recovery (cooling) signals propagating quickly from the surface to the subsurface levels (Fig. 3a).

For most of the NAtl domains, the persistence of the warming signal is an indicative of very slow recoveries within the time span of our simulation towards PI levels (Fig. 3e). We highlight that changes occurring in the South Atlantic and the Southern Ocean are potentially more pronounced and can play a key role in the redistribution of heat and its exchange at intermediate layers of the NAtl once the AMOC regains its strength.

<u>Dissolved Oxygen (DO)</u>

Our results indicate an overall deoxygenation in the upper layers of the NAtl throughout the Ramp-up, with greater ToD values than in the deeper layers, which reflect the wider envelopes associated with the high interannual variability within the mixed layer. Our results are consistent with those from *Hameau et al.* [2019] (Fig. 2a therein), who also suggest relatively higher ToD timescales for oxygen in shallower domains of the interior NAtl (<600 m), except for the regions between the centre of the subtropical gyre and the western side of the basin, where the emergence of anthropogenic signal is early due to the strong influence of the upper MOW.

Towards the deep NAtl interior, the simulated ToD values decrease, indicating the stable mesopelagic environment with respect to DO. Interestingly, departures within the upper layers were generally associated with a deoxygenation whereas for the upper mesopelagic between 500-2000 m this was not the case.

Our results show that departures can also be associated with an increase in DO that is closely linked to reduced AOU at depth. The relationship between an AOU undershoot and a DO overshoot is evident when analysing: 1) the profiles of DO and AOU Trec, where a peak of delayed Trec in AOU (between 700-1500 m) is lying just above the peak of delayed Trec for DO (between 1800-2400 m) (Fig. S7) and 2) the mean DO and AOU percentage change profiles across all the different simulation periods from the subsurface down to 2000 m (Fig. 4b and Fig. S4b), which clearly show sustained positive (negative) changes for DO (AOU). The magnitude of these changes for DO decreases chronologically after model year 250, meaning a rebound of ventilation in the upper 2000 m, whereas the magnitude of AOU percentage change did not show a trend towards PI levels and remained at constant negative values.

The combination of a DO overshoot and a constant AOU undershoot between 1000-2000 m deep after mitigation indicates that the oxygen build-up in the mesopelagic NAtl is likely a result of less oxygen utilization over time, a feature also found in other studies [*Tjiputra et al.*, 2018]. At the WH, more specifically, observational data at intermediate depths (~1200m) already show a weak oxygenation trend in this domain of the NAtl [*Oschlies et al.*, 2018]. Overall, our simulation suggests that this effect is a direct consequence of reduced EP from the surface layers to the NAtl interior (Fig. 6f), which creates a surplus of unutilized oxygen at depth when compared to the PI.

Another feature to highlight is the relatively high delay in terms of DO (and T) ToD, from 2000-3000 m and between 20-30°N. This is likely associated with shifts in the depth horizon of central water masses far west in the interior NAtl (Fig. 4c). Under a rapid anthropogenic warming, the NorESM1-ME tends to produce deeper formation zones for central water masses, such as the Western North Atlantic Central Water (WNACW), which receives input from the Mediterranean Overflow Water (MOW). *Liu and Tanhua* [2019] described that the WNACW normally occurs in the upper layer down to 1000 m. This is consistent with our results (Fig. 2), where isolines of T and DO in the interior NAtl shifted down by more than 1000 m, yielding a new depth level of ~2000 m. Additionally, by analysing both the Ttmax and DOtmax surfaces within the 500-2500 depth range against the model years in which these signals are observed (Figs. S8 and S9 respectively), it is demonstrated that this particular domain is largely influenced by warming that originates in the Mediterranean Sea.

In the phase comprising the last 30 model years of the simulation (Fig. 4e), most domains of the NAtl interior north of 40°N tend to show minor deoxygenation trends (up to -5% compared to PI levels), whereas south of 40°N in the upper mesopelagic there are still domains where significantly strong oxygenation trends of +20% can be seen, with the opposite trend in AOU for the same domain (Fig. S4e). Furthermore, the depth range of these domains increases southwards, reflecting the strong effect of remineralization rates in low and mid-latitude upper ocean water masses of the South Atlantic on DO levels of the interior NAtl, namely Antarctic Intermediate Water (AAIW). This shows that, under our simulation, the NorESM1-ME yields recoveries timescales for the South Atlantic that are significantly longer when compared to the NAtl, highlighting that DO recoveries in the low to mid-latitude domains of interior NAtl also rely on the readjustment timescales of water masses from the South Atlantic.

Between 2000-3000 m, while the AOU signal shows overall recoveries towards PI levels in the NAtl within our simulation period (Fig. S4d), DO levels show no recovery (Fig. 4d). This indicates that, even though there was a recovery with respect to the amount of oxygen being consumed for remineralization, the major factor impeding DO recovery within this depth range is the solubility effect of T prevailing in the South Atlantic, which reduces DO levels at depth even after the Extension phase (Fig. 4b and 4e).

Calcite Saturation State (Ω_c)

The basin-scale evolution of Ω_c (Fig. 2e) shows that conditions favouring calcite dissolution start to arise just before the CO_{2atm} peak in the Ramp-up phase (model year 120). Our results suggest that, under strong anthropogenic forcing, the whole NAtl experienced conditions very close to the dissolution horizon for as long as 150 years, encompassing the whole Mitigation phase (model years 140-280). This highlights the time lag between the implementation of mitigation measures and the actual response in the interior ocean.

The ToD timescales along the meridional section revealed domains of delayed departures both in the upper mesopelagic (~1000 m) and the deep ocean domains south of 30°N. These delayed departures seem to be a result of volume input from the South Atlantic, particularly due to the enhanced contribution of Antarctic Intermediate Water (AAIW) in the upper mesopelagic domain and AABW in the deep ocean, which are characterized by relatively high pH compared to already-affected NADW domain (Fig. S5c). The AAIW penetrates the NAtl mesopelagic up to ~40°N, delaying low-pH water mass penetration despite the abrupt drop in pH induced by strong atmospheric exchange at latitudes > 50°N. This indicates that one of the major processes controlling the decrease and the spread of the low Ω_c signal in the upper mesopelagic NAtl is the interplay between northward transports from the South Atlantic and the time when the AMOC slows down at subduction zones. This gradual change towards a weaker AMOC creates some latency which allows for a short-lived dominant buffering effect with respect to the penetration of a relatively high pH signal from the south. Our results also suggest that the buffering effect of AABW is less predominant if compared to the effect of AAIW in the mesopelagic. Understanding this latent relationship along with the opposing transport effects occurring at intermediate depths is crucial to projecting more precisely not only the contributions of unaltered volumes from the South Atlantic, which in turn are able to curb the low-acidity signal brought by NADW, but also improve the estimates of ToD timescales. We highlight that this dynamical feature could be model dependent and future analysis using different model systems would be valuable.

Overall, decreases in Ω_c peaked at the end of Mitigation (model years 250-280), with the volume-weighted profile for the whole NAtl from 0-65°N (Fig. 5b) showing saturation states 25% lower than PI levels for the entire mesopelagic (1000-3000 m). Furthermore, Ω_c undersaturation persists throughout the whole simulation in the upper mesopelagic between 500-1500 m (Fig. 2e), meaning unlikely recoveries in that zone even after the Extension phase. However, when the extent of recovery along the meridional section is examined, a distinct separation is seen at the latitude of 35°N. Most domains in the interior NAtl north of 35°N showed recoveries within the last 30 years of the simulation and even some minor Ω_c overshoots between 1000-2000 m, likely linked to the re-introduction of relatively high-pH water masses from other regions. Conversely, south of 35°N significant undershoots are still present and are pronounced in domains that are influenced by intermediate and deep water masses from the South Atlantic, such as AAIW (~1000 m) and AABW (>3500 m) respectively. This indicates that the anthropogenic disturbance is still propagating within the South Atlantic as a persisting decrease in pH which is reflected in the Ω_c signal in the NAtl interior (Fig. S5e).

Unlike what has been observed for the departure timescales associated with T and DO, ToD values for Ω_c did not form a cluster of delayed departures in the domain characterized by the influence of the MOW (Fig. 5b, ~30°N). This shows that anthropogenic disturbances altering the Ω_c signal in the Mediterranean are readily cascading through the mid-latitude zones of central water masses in the NAtl. Interestingly, while a cluster of delayed recoveries cannot be observed for T at the domain dominated by intermediate-depth water masses, as late recoveries seem to be widespread over the interior NAtl, our results revealed the presence MOW-related clusters of delayed Trec for both DO and Ω_c (Fig. 4d and 5d). However, their depth range differs, with the DO cluster appearing at a shallower position (~1000 m) when compared with that of Ω_c ~1500 m. This disparity in depth horizon can partially be due to changes in biological activity and a consequence of enhanced EP (see below), which initially induces high remineralization at intermediate levels and causes a subsequent injection of DIC at deeper levels, therefore decreasing overall pH and sustaining a net decrease in Ω_c.

Export Production (EP)

Our results reveal a generalised spread of low-production zones, especially on the western side of the NAtl subtropical gyre. Eastwards, decreases are also noticeable when we take into account the contrast between the PI mean and EP_{tmax} (Fig. 6a and 6b), with widespread decreases along the European shelf (45°N,10°W) as well as a significant reduction over the Canary upwelling system (22°N,18°W). However, some patches of localized increase in export production were also observed, especially in parts of the Irminger Sea and the domain from the Reykjanes Ridge to the Azores, which are associated with relatively later ToD values (>250 model years, Fig. 6c).

There is little variation in both zonally-averaged EP ToD and Trec, indicating that, at the domains where departures were observed, significant changes in export production will occur no later than ~10 years into the Mitigation phase with a general trend towards earlier departures in higher latitudes (Fig. 6c and 6e).

The last 30 model years of the simulation reveal a scenario of predominant decrease in export production except for the WH area in the subpolar region, where trends towards cooling, oxygenation and increased EP were detected at the end of the simulation. The increases in DO and EP signals seem to result from enhanced instability in the water column caused by the decrease in T, which deepens the mixed layer depth (MLD), favouring productive regimes as well as enhanced ventilation.

5. Conclusion

Despite applying symmetrical forcing (i.e., a CO_2 ramp-up of +1% yr^{-1} followed by a CO_2 ramp down -1% yr^{-1}), our study reveals that the responses observed in the interior NAtl in terms of physical and biogeochemical drivers were asymmetric, with strong spatial variations that remained even after allowing for stabilization over the Extension phase. Our study highlights that vast regions in the interior NAtl, especially the mesopelagic, tend to respond to anthropogenic forcing significantly earlier than domains in the subsurface. It is also in these regions of early departure that recovery timescales are most affected, meaning that in regions of relatively rapid change the recovery is even slower. When looking at individual parameters, Temperature data revealed overall unlikely recoveries in the interior NAtl towards PI levels. At the end of the experiment, mesopelagic regions displayed modest cooling in response to decreased anthropogenic forcing but remained 15% warmer than the PI on average. Conversely, instead of cooling, our data suggests that Temperature in domains of the deep NAtl were progressively warm throughout all the simulation phases. This suggests that domains in the South Atlantic and Southern Ocean accumulated heat as the AMOC slowed down over the Ramp-up. Once the AMOC regained some of its strength, this heat surplus started to be exchanged across the Atlantic, consequently affecting readjustment timescales over the entire deep NAtl as far as 50°N.

With respect to oxygen, our data suggests a pattern of rather counterintuitive oxygenation despite the anthropogenic warming in the mesopelagic NAtl. This oxygen overshoot is linked to a decrease in biological remineralization, which is caused by a decrease in export production from the surface layers. This ultimately translates into a reduction in the organic matter exported to the interior, creating a surplus of unutilized oxygen relative to the PI. Regarding Ω_c, our simulation suggests that departure timescales in the upper mesopelagic NAtl are closely linked to changes in pH and mediated by the northward transports from the South Atlantic and the gradual attenuation of the AMOC. This interplay allows for a short-lived dominant buffering with respect to the penetration of a relatively high-pH signal from the south at intermediate depths. This buffering effect, however, seems to be stronger in the domains influenced by AAIW when compared to the domain of the AABW. Further investigations on how these opposing transports, which counteract the acidity signal from NADW, affect timescales of climate change are crucial to improve our understanding of how relatively unaltered volumes from the South Atlantic have an impact on ToD timescales in the mesopelagic NAtl. We emphasize that this dynamical interplay could be a model-dependent feature and further studies using different models would be valuable.

Here we show that, for variables which revealed likely recoveries within the timeframe of the simulation, recovery timescales in the NAtl interior are out of phase (i.e., not concurrent). For example, the layered structure of delayed Trec values for DO and Ωc at mid latitudes reveals that different recovery signals are associated with a Mediterranean Overflow that is not biogeochemically homogeneous and, thus, an indicative of out-of-phase recoveries occurring at different domains within the Mediterranean Sea. Additionally, our results indicate that both the Mediterranean overflow as well as other intermediate-depth processes regulating water mass restructuring are key in controlling the recovery of calcite saturation in mid-latitudes of the mesopelagic NAtl. Further studies focused on the impacts of biogeochemical shifts not only in the Mediterranean Overflow but also other important processes that form mid-latitude water masses are needed to better understand the impacts on the biogeochemistry of the mesopelagic North Atlantic under climate change.

Improving how export production is represented in the models is valuable to understand whether the features observed here arise from adopting a relatively shallow layer, where productivity is confined to the first 100 m and the recycling of organic matter is not mediated by an explicit microbial loop. Furthermore, a more robust representation of the lower trophic ecosystem processes and the adoption of our method using other ESMs can improve our understanding of any simulated counterintuitive patterns (e.g. the oxygen overshoot in the mesopelagic NAtl followed by warming and the WH region characterized by cooling and enhanced EP). Such exercise can help us determine, for example, whether the oxygen overshoot detected here is a model caveat or an actual indication of the solubility effect being surpassed by biological activity under extreme climate change. Moreover, the use of more realistic climate change and mitigation scenarios in such studies, e.g., SSP5-3.4, can ultimately help shed new light on where the threshold lies in terms of the amount of change that is necessary for the solubility effect to become less important in controlling DO levels in the NAtl interior.

We highlight that future studies focused on the relationship between AMOC strength, changes in ocean biogeochemistry and their effects on ToD and Trec timescales in the deep ocean are needed to better understand how these properties are linked and how they translate into exposure horizons beyond which significant changes in marine assemblages are expected. The existing studies that have modelled timing of climate change emergence (i.e., ToD) as well as timing of exposure to conditions beyond niche limits are scarce for marine species, mostly confined to the epipelagic zone and have focused on changes in terms of temperature. We currently lack more integrative approaches involving the covarying and synergistic effects of biogeochemical variables on ecosystem function, which can constrain species range and their tolerance to climate change scenarios even more [*Coll et al.*, 2020; *Trisos et al.*, 2020].

To conclude, we reiterate that it is time for the community to start focusing not just on changes to the marine environment in the epipelagic zone given how vast, biogeochemically active and interconnected the various domains of the deep NAtl are. The results shown here come from a single model and it would be invaluable to test the robustness of our results using other models. At the time of our study, the CMIP6 model CDRMIP simulations were not available. Holistic modelling exercises on how covarying shifts in biogeochemical drivers can be used as proxies for changes in deep-ocean marine assemblages are key to better inform policy making. Such studies can ultimately aid in our understanding of how exposure times can affect carbon and nutrient recycling at depth, water mass restructuring, as well as species distribution and ultimately help better project the consequences of extreme climate change scenarios for the deep ocean.

6. Acknowledgements

We would like to acknowledge the Norwegian Research Council funded projects ORGANIC (Overturning circulation and its implications for global carbon cycle in coupled model; № 239965) THRESHOLDS (Thresholds for destabilizing thermohaline circulation and ocean carbon cycling in a warmer world; № 254964), and COLUMBIA (Constraining the Large Uncertainties in Earth System Model Projections with a Big Data Approach; № 275268). This study has been carried out as part of the IMBRSea Erasmus+: Erasmus Mundus Joint Master’s Degree (EMJMD) Programme and supported by an EMJMD Scholarship, under the EU Grant Agreement № 2016-2280. The NorESM1-ME ramp-up simulation output is publicly available at the CMIP5 repository: https://esgf-data.dkrz.de/projects/esgf-dkrz/. Fully coupled ramp-down and

extension simulations are long-term archived at the NorStore Research Data Archive and can be accessed under https://doi.org/10.11582/2018.00011.

7. References

Assmann, K., M. Bentsen, C. Heinze, and J. Segschneider (2010), An isopycnic ocean carbon cycle model, *Geoscientific Model Development*, *3*, 143-167.

Baillon, S., J.-F. Hamel, V. E. Wareham, and A. Mercier (2012), Deep cold-water corals as nurseries for fish larvae, *Frontiers in Ecology and the Environment*, *10*(7), 351-356.

Bentsen, M., I. Bethke, J. Debernard, T. Iversen, A. Kirkevåg, Ø. Seland, H. Drange, C. Roelandt, I. Seierstad, and C. Hoose (2013), The Norwegian earth system model, NorESM1-M—Part 1: Description and basic evaluation of the physical climate, *Geosci. Model Dev*, *6*(3), 687-720.

Boucher, O., P. Halloran, E. Burke, M. Doutriaux-Boucher, C. Jones, J. Lowe, M. Ringer, E. Robertson, and P. Wu (2012), Reversibility in an Earth System model in response to CO_2 concentration changes, *Environmental Research Letters*, *7*(2), 024013.

Box, J., X. Fettweis, J. Stroeve, M. Tedesco, D. Hall, and K. Steffen (2012), Greenland ice sheet albedo feedback: thermodynamics and atmospheric drivers, *The Cryosphere*, *6*(4), 821-839.

Buhl-Mortensen, L., S. H. Olafsdottir, P. Buhl-Mortensen, J. M. Burgos, and S. A. Ragnarsson (2015), Distribution of nine cold-water coral species (Scleractinia and Gorgonacea) in the cold temperate North Atlantic: effects of bathymetry and hydrography, *Hydrobiologia*, *759*(1), 39-61.

Caesar, L., S. Rahmstorf, and G. Feulner (2020), On the relationship between Atlantic meridional overturning circulation slowdown and global surface warming, *Environmental Research Letters*, *15*(2), 024003.

Chen, X., and K.-K. Tung (2018), Global surface warming enhanced by weak Atlantic overturning circulation, *Nature*, *559*(7714), 387.

Coll, M., J. Steenbeek, M. G. Pennino, J. Buszowski, K. Kaschner, H. K. Lotze, Y. Rousseau, D. P. Tittensor, C. Walters, and R. A. Watson (2020), Advancing Global Ecological Modeling Capabilities to Simulate Future Trajectories of Change in Marine Ecosystems, *Frontiers in Marine Science*, *7*, 741.

Costello, M. J., M. McCrea, A. Freiwald, T. Lundälv, L. Jonsson, B. J. Bett, T. C. van Weering, H. de Haas, J. M. Roberts, and D. Allen (2005), Role of cold-water Lophelia pertusa coral reefs as fish habitat in the NE Atlantic, in *Cold-water corals and ecosystems*, edited, pp. 771-805, Springer.

Courtney, T. A., et al. (2017), Environmental controls on modern scleractinian coral and reef-scale calcification, *Science Advances*, *3*(11), e1701356, doi:10.1126/sciadv.1701356.

Drijfhout, S., G. J. v. Oldenborgh, and A. Cimatoribus (2012), Is a Decline of AMOC Causing the Warming Hole above the North Atlantic in Observed and Modeled Warming Patterns?, *Journal of Climate*, *25*(24), 8373-8379, doi:10.1175/jcli-d-12-00490.1.

Friedlingstein, P., R. M. Andrew, J. Rogelj, G. P. Peters, J. G. Canadell, R. Knutti, G. Luderer, M. R. Raupach, M. Schaeffer, and D. P. van Vuuren (2014), Persistent growth of CO_2 emissions and implications for reaching climate targets, *Nature geoscience*, *7*(10), 709-715.

Garcia, H., R. Locarnini, T. Boyer, J. Antonov, M. Zweng, O. Baranova, and D. Johnson (2010a), World Ocean Atlas 2009, edited, Volume.

Garcia, H., R. Locarnini, T. Boyer, J. Antonov, M. Zweng, O. Baranova, and D. Johnson (2010b), World Ocean Atlas 2009, vol. 4, Nutrients (Phosphate, Nitrate, Silicate), edited by: Levitus, S, *NOAA Atlas NESDIS, US Gov. Printing Office, Wash., DC*, *71*.

Gasser, T., C. Guivarch, K. Tachiiri, C. Jones, and P. Ciais (2015), Negative emissions physically needed to keep global warming below 2 C, *Nature communications*, *6*(1), 1-7.

Gehlen, M., R. Séférian, D. O. Jones, T. Roy, R. Roth, J. Barry, L. Bopp, S. C. Doney, J. P. Dunne, and C. Heinze (2014), Projected pH reductions by 2100 might put deep North Atlantic biodiversity at risk, *Biogeosciences*, *11*(23), 6955-6967.

Goris, N., J. Tjiputra, J. Schwinger, and C. Heinze (2015), Responses of carbon uptake and oceanic pCO_2 to climate change in the North Atlantic: A model study with the Bergen Earth System Model, *Global Biogeochemical Cycles*, *29*(10), 1567-1583.

Guinotte, J. M., J. Orr, S. Cairns, A. Freiwald, L. Morgan, and R. George (2006), Will human-induced changes in seawater chemistry alter the distribution of deep-sea scleractinian corals?, *Frontiers in Ecology and the Environment*, *4*(3), 141-146, doi:10.1890/1540-9295(2006)004[0141:Whcisc]2.0.Co;2.

Hameau, A., J. Mignot, and F. Joos (2019), Assessment of time of emergence of anthropogenic deoxygenation and warming: insights from a CESM simulation from 850 to 2100 CE, *Biogeosciences*, *16*, 1755-1780.

Hebbeln, D., R. d. C. Portilho-Ramos, C. Wienberg, and J. Titschack (2019), The Fate of Cold-Water Corals in a Changing World: A Geological Perspective, *Frontiers in Marine Science*, *6*(119), doi:10.3389/fmars.2019.00119.

Hennige, S. J., L. C. Wicks, N. A. Kamenos, G. Perna, H. S. Findlay, and J. M. Roberts (2015), Hidden impacts of ocean acidification to live and dead coral framework, *Proceedings of the Royal Society B: Biological Sciences*, *282*(1813), 20150990, doi:doi:10.1098/rspb.2015.0990.

Henry, L.-A., J. M. Navas, S. J. Hennige, L. C. Wicks, J. Vad, and J. M. Roberts (2013), Cold-water coral reef habitats benefit recreationally valuable sharks, *Biological conservation*, *161*, 67-70.

Henson, S. A., C. Beaulieu, T. Ilyina, J. G. John, M. Long, R. Seferian, J. Tjiputra, and J. L. Sarmiento (2017), Rapid emergence of climate change in environmental drivers of marine ecosystems, *Nature Communications*, *8*, doi:10.1038/ncomms14682.

Hidalgo, M., and H. I. Browman (2019), Developing the knowledge base needed to sustainably manage mesopelagic resources, edited, Oxford University Press.

Hofmann, M., S. Mathesius, E. Kriegler, D. van Vuuren, and H. Schellnhuber (2019), Strong time dependence of ocean acidification mitigation by atmospheric carbon dioxide removal, *Nature Communications*, *10*(1), 1-10.

IPCC, 2019: Summary for Policymakers. In: IPCC Special Report on the Ocean and Cryosphere in a Changing Climate [H.-O. Pörtner, D.C. Roberts, V. Masson-Delmotte, P. Zhai, M. Tignor, E. Poloczanska, K. Mintenbeck, A. Alegría, M. Nicolai, A. Okem, J. Petzold, B. Rama, N.M. Weyer (eds.)]. In press

Irigoien, X., T. A. Klevjer, A. Røstad, U. Martinez, G. Boyra, J. Acuña, A. Bode, F. Echevarria, J. I. González-Gordillo, and S. Hernandez-Leon (2014), Large mesopelagic fishes biomass and trophic efficiency in the open ocean, *Nature communications*, *5*, 3271.

Jones, D. O., A. Yool, C. L. Wei, S. A. Henson, H. A. Ruhl, R. A. Watson, and M. Gehlen (2014), Global reductions in seafloor biomass in response to climate change, *Global change biology*, *20*(6), 1861-1872.

Keeling, C. D., S. C. Piper, R. B. Bacastow, M. Wahlen, T. P. Whorf, M. Heimann, and H. A. Meijer (2005), Atmospheric CO_2 and $^{13}CO_2$ Exchange with the Terrestrial Biosphere and Oceans from 1978 to 2000: Observations and Carbon Cycle Implications, in *A History of Atmospheric CO_2 and Its Effects on Plants, Animals, and Ecosystems*, edited by I. T. Baldwin, et al., pp. 83-113, Springer New York, New York, NY, doi:10.1007/0-387-27048-5_5.

Keller, F. Joos, and C. Raible (2014), Time of emergence of trends in ocean biogeochemistry, *Biogeosciences*, *11*(13), 3647-3659.

Keller, D. P., A. Lenton, V. Scott, N. E. Vaughan, N. Bauer, D. Ji, C. D. Jones, B. Kravitz, H. Muri, and K. Zickfeld (2018), The carbon dioxide removal model intercomparison project (CDRMIP): rationale and experimental protocol for CMIP6, *Geoscientific Model Development*, *11*(3), 1133-1160.

Key, R. M., A. Kozyr, C. L. Sabine, K. Lee, R. Wanninkhof, J. L. Bullister, R. A. Feely, F. J. Millero, C. Mordy, and T. H. Peng (2004), A global ocean carbon climatology: Results from Global Data Analysis Project (GLODAP), *Global Biogeochem. Cycles*, *18*(4).

Kirkevåg, A., T. Iversen, Ø. Seland, C. Hoose, J. Kristjánsson, H. Struthers, A. Ekman, S. Ghan, J. Griesfeller, and E. Nilsson (2012), Aerosol-climate interactions in the Norwegian Earth System Model–NorESM, *Geoscientific Model Development Discussions*, *5*(3), 2599-2685.

Kwiatkowski, L., O. Torres, L. Bopp, O. Aumont, M. Chamberlain, J. R. Christian, J. P. Dunne, M. Gehlen, T. Ilyina, and J. G. John (2020), Twenty-first century ocean warming, acidification, deoxygenation, and upper-ocean nutrient and primary production decline from CMIP6 model projections, *Biogeosciences*, *17*(13), 3439-3470.

Levin, L. A., and N. Le Bris (2015), The deep ocean under climate change, *Science*, *350*(6262), 766-768, doi:10.1126/science.aad0126.

Liu, M., and T. Tanhua (2019), Distribution of Water Masses in the Atlantic Ocean based on GLODAPv2, *Ocean Science Discussions*, 1-32.

Mahowald, N. M., A. R. Baker, G. Bergametti, N. Brooks, R. A. Duce, T. D. Jickells, N. Kubilay, J. M. Prospero, and I. Tegen (2005), Atmospheric global dust cycle and iron inputs to the ocean, *Global biogeochemical cycles*, *19*(4).

Maier-Reimer, E. (1993), Geochemical cycles in an ocean general circulation model. Preindustrial tracer distributions, *Global Biogeochemical Cycles*, *7*(3), 645-677.

McDougall, T. J., and P. M. Barker (2011), Getting started with TEOS-10 and the Gibbs Seawater (GSW) oceanographic toolbox, *SCOR/IAPSO WG*, *127*, 1-28.

Meyer, J., and U. Riebesell (2015), Reviews and Syntheses: Responses of coccolithophores to ocean acidification: a meta-analysis, *Biogeosciences*, *12*(6), 1671-1682, doi:10.5194/bg-12-1671-2015.

Oschlies, A., P. Brandt, L. Stramma, and S. Schmidtko (2018), Drivers and mechanisms of ocean deoxygenation, *Nature Geoscience*, *11*(7), 467-473.

Puerta, P., C. Johnson, M. Carreiro-Silva, L.-A. Henry, E. Kenchington, T. Morato, G. Kazanidis, J. L. Rueda, J. Urra, and S. Ross (2020), Influence of Water Masses on the Biodiversity and Biogeography of Deep-Sea Benthic Ecosystems in the North Atlantic, *Frontiers in Marine Science*, *7*, 239.

Ramirez-Llodra, E., P. A. Tyler, M. C. Baker, O. A. Bergstad, M. R. Clark, E. Escobar, L. A. Levin, L. Menot, A. A. Rowden, and C. R. Smith (2011), Man and the last great wilderness: human impact on the deep sea, *PLoS one*, *6*(8), e22588.

Riebesell, U., et al. (2018), Toxic algal bloom induced by ocean acidification disrupts the pelagic food web, *Nature Climate Change*, *8*(12), 1082-1086, doi:10.1038/s41558-018-0344-1.

Sarmiento, J. L., and C. Le Quere (1996), Oceanic carbon dioxide uptake in a model of century-scale global warming, *Science*, *274*(5291), 1346-1350.

Schwinger, J., and J. Tjiputra (2018), Ocean carbon cycle feedbacks under negative emissions, *Geophysical Research Letters*, *45*(10), 5062-5070.

Smeed, D., G. McCarthy, S. Cunningham, E. Frajka-Williams, D. Rayner, W. E. Johns, C. Meinen, M. Baringer, B. Moat, and A. Duchez (2014), Observed decline of the Atlantic meridional overturning circulation 2004–2012, *Ocean Science*, *10*(1), 29-38.

Smith, P., S. J. Davis, F. Creutzig, S. Fuss, J. Minx, B. Gabrielle, E. Kato, R. B. Jackson, A. Cowie, and E. Kriegler (2016), Biophysical and economic limits to negative CO 2 emissions, *Nature climate change*, *6*(1), 42-50.

Steffen, W., J. Rockström, K. Richardson, T. M. Lenton, C. Folke, D. Liverman, C. P. Summerhayes, A. D. Barnosky, S. E. Cornell, and M. Crucifix (2018), Trajectories of the Earth System in the Anthropocene, *Proceedings of the National Academy of Sciences*, *115*(33), 8252-8259.

Tjiputra, K. Assmann, M. Bentsen, I. Bethke, O. Otterå, C. Sturm, and C. Heinze (2010a), Bergen Earth system model (BCM-C): model description and regional climate-carbon cycle feedbacks assessment, *Geoscientific Model Development*, *3*(1), 123-141.

Tjiputra, K. Assmann, and C. Heinze (2010b), Anthropogenic carbon dynamics in the changing ocean, *Ocean Science*, *6*(3), 605.

Tjiputra, N. Goris, S. K. Lauvset, C. Heinze, A. Olsen, J. Schwinger, and R. Steinfeldt (2018), Mechanisms and Early Detections of Multidecadal Oxygen Changes in the Interior Subpolar North Atlantic, *Geophysical Research Letters*, *45*(9), 4218-4229, doi:10.1029/2018gl077096.

Tjiputra, C. Roelandt, M. Bentsen, D. M. Lawrence, T. Lorentzen, J. Schwinger, O. Seland, and C. Heinze (2013), Evaluation of the carbon cycle components in the Norwegian Earth System Model (NorESM), *Geoscientific Model Development*, *6*(2), 301-325, doi:10.5194/gmd-6-301-2013.

Tokarska, K. B., and K. Zickfeld (2015), The effectiveness of net negative carbon dioxide emissions in reversing anthropogenic climate change, *Environmental Research Letters*, *10*(9), 094013.

Trisos, C. H., C. Merow, and A. L. Pigot (2020), The projected timing of abrupt ecological disruption from climate change, *Nature*, *580*(7804), 496-501.

Völker, C., D. W. Wallace, and D. A. Wolf-Gladrow (2002), On the role of heat fluxes in the uptake of anthropogenic carbon in the North Atlantic, *Global biogeochemical cycles*, *16*(4), 85-81-85-89.

Wassmann, P., C. M. Duarte, S. Agusti, and M. K. Sejr (2011), Footprints of climate change in the Arctic marine ecosystem, *Global change biology*, *17*(2), 1235-1249.

Webster, N. S., A. P. Negri, E. S. Botté, P. W. Laffy, F. Flores, S. Noonan, C. Schmidt, and S. Uthicke (2016), Host-associated coral reef microbes respond to the cumulative pressures of ocean warming and ocean acidification, *Scientific Reports*, *6*, 19324, doi:10.1038/srep19324
https://www.nature.com/articles/srep19324#supplementary-information.

Zickfeld, K., M. Eby, and A. J. Weaver (2008), Carbon-cycle feedbacks of changes in the Atlantic meridional overturning circulation under future atmospheric CO2, *Global Biogeochemical Cycles*, *22*(3).